

## A Class of the van Leer-type Transport Schemes and Its Application to the Moisture Transport in a General Circulation Model

SHIAN-JIANN LIN,\* WINSTON C. CHAO, Y. C. SUD, AND G. K. WALKER\*

*Laboratory for Atmospheres, NASA/Goddard Space Flight Center, Greenbelt, Maryland*

(Manuscript received 15 February 1993, in final form 15 November 1993)

### ABSTRACT

A generalized form of the second-order van Leer transport scheme is derived. Several constraints to the implied subgrid linear distribution are discussed. A very simple positive-definite scheme can be derived directly from the generalized form. A monotonic version of the scheme is applied to the Goddard Laboratory for Atmospheres (GLA) general circulation model (GCM) for the moisture transport calculations, replacing the original fourth-order center-differencing scheme. Comparisons with the original scheme are made in idealized tests as well as in a summer climate simulation using the full GLA GCM. A distinct advantage of the monotonic transport scheme is its ability to transport sharp gradients without producing spurious oscillations and unphysical negative mixing ratio. Within the context of low-resolution climate simulations, the aforementioned characteristics are demonstrated to be very beneficial in regions where cumulus convection is active. The model-produced precipitation pattern using the new transport scheme is more coherently organized both in time and in space, and correlates better with observations. The side effect of the filling algorithm used in conjunction with the original scheme is also discussed, in the context of idealized tests.

The major weakness of the proposed transport scheme with a local monotonic constraint is its substantial implicit diffusion at low resolution. Alternative constraints are discussed to counter this problem.

### 1. Introduction

Monotonic upstream-biased transport schemes have received greater attention among mesoscale modelers. Application of monotonic schemes such as Smolarkiewicz's scheme (Smolarkiewicz and Grabowski 1990), Multidimensional flux-corrected transport (Zalesak 1979) by Xue and Thorpe (1991), and van Leer's scheme (van Leer 1977 and 1979) and its variant piecewise parabolic method (PPM), (Colella and Woodward 1984) by Carpenter et al. (1990) to mesoscale problems are in general very successful. The upstream Lagrangian nature of these schemes implies that they are generally diffusive. The imposed monotonic constraint further prevents overshoots and undershoots from developing, and consequently, no spurious oscillations can occur, and the positive definiteness of the transported constituent is automatically maintained. These schemes can be applied to scalars only (potential temperature and water substances) (Xue and Thorpe 1991) or to all prognostic variables (Carpenter et al.

1990; Smolarkiewicz and Margolin 1993). In this paper, we will study their application to passive scalars in a 3D global model, with water substances particularly in mind.

Most of the published monotonic transport schemes are formulated for the local Cartesian coordinate in finite-difference form. Due to the singular nature of the spherical coordinate system near poles, implementation of these schemes in a 3D global model is not straightforward and is often impractical. Semi-Lagrangian advection schemes formulated specifically for the spherical geometry (e.g., Williamson and Rasch 1989; Smolarkiewicz and Rasch 1991) are very efficient when large time steps can be taken, but this advantage is partially lost when coupled to an Eulerian model (Williamson 1990; Rasch and Williamson 1991), and the nonconservation of total mass could potentially become a problem for long-term climate simulations. Smolarkiewicz's multidimensional scheme (Smolarkiewicz 1984; Smolarkiewicz and Grabowski 1990; Smolarkiewicz and Rasch 1991) formulated on the sphere is conservative. Unfortunately, the largest time step allowed is limited by a very small grid size in the zonal direction near the poles, and the lower-order scheme is diffusive, whereas the less diffusive higher-order version is expensive as compared to its nonconservative semi-Lagrangian counterpart (Smolarkiewicz and Rasch 1991).

\* Also affiliated with General Sciences Corp., Laurel, Maryland, a subsidiary of Science Applications International Corp.

Corresponding author address: Dr. Shian-Jiann Lin, General Sciences Corp., Code 910.3, NASA/Goddard Space Flight Center, Greenbelt, MD 20771.

A different approach was taken by Allen et al. (1991, ADRG hereafter). Instead of taking the semi-Lagrangian approach to overcome the pole problem, a strictly 1D van Leer scheme is applied to perform the 3D global transport of ozone by means of time splitting. Their implementation of a second-order van Leer scheme is simple and efficient. There is no need for an explicit "spatial filter" (or as sometimes called "sub-grid-scale turbulence parameterization") to account for numerical deficiencies and a filling algorithm to eliminate negative mixing ratio. Consequently, the monotone scheme is able to maintain a better constituent correlation as compared to the global spectral method. Zonal transport at high latitudes is split in time to satisfy local Courant–Friedrichs–Lewy (CFL) condition. The large time step applied at low latitudes and in other spatial directions is therefore comparable to that of a global spectral model at comparable resolution.

Thuburn (1993) obtained very encouraging results using a van Leer–type scheme for the vertical transport in a global circulation model. Williamson (1990) and Rasch and Williamson (1991) applied the 3D shape-preserving semi-Lagrangian scheme to global spectral models for moisture transport with also very positive results. Since the time step is still limited by the Eulerian model dynamics and only one variable is predicted, the semi-Lagrangian approach is not very efficient. As previously mentioned, a potential problem with traditional semi-Lagrangian advection schemes is that total moisture (mass) is not conserved. As studied by Takacs (1988) and discussed by Rasch and Williamson (1991), an a posteriori procedure to restore conservation properties is not likely to improve the overall accuracy. On the other hand, a van Leer–type scheme can be viewed as a conservative 1D Lagrangian scheme (Colella and Woodward 1984) and, indeed, can be formulated as such. To apply a van Leer–type scheme to the moisture transport in a general circulation model (GCM) with an explicit time integration scheme, the simpler Eulerian approach of ADRG should be chosen. That is, instead of a Lagrangian formulation in the zonal direction, we shall apply time splitting at high latitudes to alleviate the time-step restriction associated with the converging meridians. In practice, as discussed in section 2, the overhead associated with this time-splitting approach is very small. Although it is known that time or directional splitting could introduce additional errors (see, for example, Smolarkiewicz 1984), this error is scheme dependent, and van Leer–type schemes (including PPM) have not been known to be susceptible to this error in multidimensional simulations. [See the discussion in Carpenter et al. (1990) and the review article by Woodward and Colella (1984).] For the Goddard Laboratory for Atmospheres (GLA) GCM, which uses an explicit time integration scheme (leapfrog or Matsuno), the time step is limited by the fastest propagating wave in the

system, not just the largest advection speed. It is therefore necessary to apply a polar filter to tendency terms of all prognostic variables (zonal and meridional momentum, surface pressure, potential temperature, and water vapor mixing ratio). When moisture transport is replaced by van Leer's scheme, there is no need for polar filtering, which would introduce error of its own. [See Takacs and Balgovich (1983) for a discussion on the side effects of the polar filter.] Since the integration time step is relatively small in an explicit gridpoint model, such as the GLA GCM, time and directional splitting error in the moisture transport using van Leer's scheme is expected to be negligibly small compared to other time and space truncation errors in the model. The need to perform time and/or directional splitting with a van Leer–type scheme is therefore not necessarily a drawback.

It is demonstrated in this study that, despite the strong coupling between the moisture field and other dynamic variables through parameterized moist processes (i.e., cumulus convection, evaporation, and large-scale condensation), a van Leer–type monotonic scheme can be advantageously used for the moisture transport in a GCM. We accomplish this by simply replacing the original finite-difference code in the GLA GCM for water vapor transport with a second-order van Leer's scheme. All filters previously applied to the moisture field except vertical turbulent fluxes, which include the flux of the water vapor (due to evaporation) from the earth's surface, are removed. Owing to the use of a more relaxed monotonic constraint, this implementation of van Leer's transport scheme is less diffusive and therefore more accurate than that of ADRG for their ozone transport calculations. In addition, the unnecessary well-mixed polar caps assumption is removed. Unlike the implementation of ADRG, the vertical velocity calculation in the original code does not need to be modified to ensure mass conservation.

The organization of this paper is as follows. A generalized form of the van Leer scheme is derived in section 2. Positive-definite-only or truly monotonic schemes are derived directly from this general form. Implementation of the scheme on the sphere is also given there. Idealized tests as well as a comparison in full GCM simulations are presented in section 3; these are followed by summary and concluding remarks in the final section.

## 2. A class of the van Leer–type schemes and its implementation to a GCM

We shall consider the general formulation of the transport (advection) of the density distribution of a scalar in one spatial direction with variable resolution. Transport in multidimensions is achieved by alternating directional splitting. We define  $\bar{\Phi}_{i+1/2}$  as the *mean* (in space) density inside the cell bounded by  $x_i$  and  $x_{i+1}$ . It is assumed that the *subgrid* distribution of  $\Phi$  is linear.

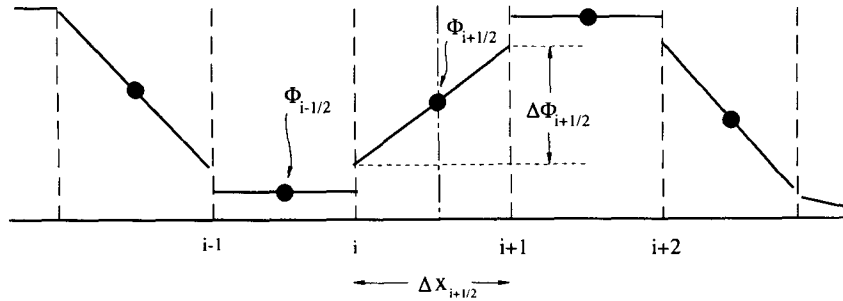


FIG. 1. Subgrid linear distribution of the second-order van Leer scheme. The cell averages are denoted by black dots. Mismatch is defined as the difference between right and left edges of a cell.

Given the “mismatch”  $\Delta\Phi_{i+1/2}$  (the difference between  $\Phi$  at right and left edges of a cell, see Fig. 1) and the mean  $\Phi_{i+1/2}$ , the subgrid distribution between  $x_i$  and  $x_{i+1}$  is uniquely defined. It is important to note that the subgrid density distribution does not need to be continuous across cell boundaries.

We shall consider only formulation in the Eulerian space. Assuming that the Courant number ( $C = U\Delta t / \Delta x$ ) is less than unity everywhere, the original distribution is transported downstream one time step  $\Delta t$ , as illustrated in Fig. 2 (a and b, for  $U_i \geq 0$  and  $U_i < 0$ ,

respectively). From mass conservation, we obtain the following discretized flux form representation of the transport equation for the cell-average density distribution:

$$\Phi_{i+1/2}^{n-1} = \Phi_{i+1/2}^n - \frac{\Delta t}{\Delta x_{i+1/2}} [\text{FLUX}_{(i+1)} - \text{FLUX}_{(i)}], \tag{1a}$$

where  $\text{FLUX}_{(i)}$  is the time rate of mass transfer across the cell interface at  $x_i$  from the upstream direction:

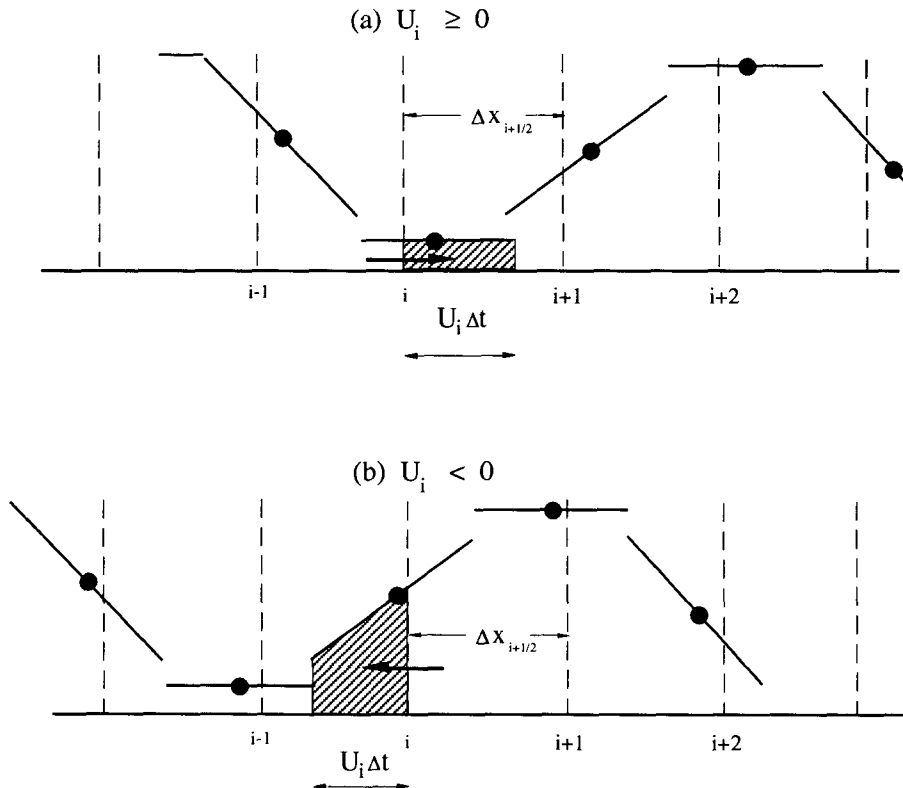


FIG. 2. Flux evaluation for (a)  $U_i \geq 0$  and (b)  $U_i < 0$ . The shaded region represents the total mass transfer across  $x_i$  from the upstream direction.

$$\text{FLUX}_{(i)} = U_i \left[ \Phi_{i-1/2}^n + \frac{\Delta\Phi_{i-1/2}}{2} (1 - C_i^-) \right],$$

for  $U_i \geq 0$  (1b)

$$\text{FLUX}_{(i)} = U_i \left[ \Phi_{i+1/2}^n - \frac{\Delta\Phi_{i+1/2}}{2} (1 + C_i^+) \right],$$

for  $U_i < 0$  (1c)

$$C_i^- = \frac{U_i \Delta t}{\Delta x_{i-1/2}}, \quad C_i^+ = \frac{U_i \Delta t}{\Delta x_{i+1/2}};$$

$U_i$  is the velocity defined at  $x_i$ ,  $n$  is the time step index, and  $C_i^-$  and  $C_i^+$  stand for the upwind Courant number. The determination of the mismatch (or, equivalently, the slope of the subgrid linear distribution) is crucial to the overall accuracy of the scheme. Note that the above scheme degenerates to the familiar first-order upstream scheme if we set  $\Delta\Phi_{i+1/2} = 0$ , for all  $i$ . At this point, the most natural choice of the mismatch appears to be the algebraic mean of the two one-sided differences of the cell-mean density; that is,

$$[\Delta\Phi_{i+1/2}]_{\text{avg}} = \frac{\delta\Phi_i + \delta\Phi_{i+1}}{2}, \quad (2)$$

where

$$\delta\Phi_i = \Phi_{i+1/2}^n - \Phi_{i-1/2}^n.$$

The scheme represented by (1) and (2) is a second-order-accurate upstream-biased scheme. Unfortunately, it guarantees neither monotonicity nor positive definiteness. To achieve either, the magnitude of the mismatch as given by (2) must be limited in some appropriate way. For example, if a local lower bound  $\Phi_{i+1/2}^{\min}$  on  $\Phi_{i+1/2}$  (the cell-mean distribution) is desired, one could limit the mismatch such that

$$\Delta\Phi_{i+1/2} = \text{sign}([\Delta\Phi_{i+1/2}]_{\text{avg}}) \min\{ |[\Delta\Phi_{i+1/2}]_{\text{avg}}|, 2 \text{ DIM}(\Phi_{i+1/2}, \Phi_{i+1/2}^{\min}) \}, \quad (3a)$$

where  $\text{DIM}(x_1, x_2)$  is defined as the positive difference between the first argument  $x_1$  and the second argument  $x_2$  (as the standard American National Standards Institute Fortran function). By simply setting  $\Phi_{i+1/2}^{\min}$  in (3a) to zero and assuming the distribution is initially positive definite, we obtain the following surprisingly simple positive-definite constraint:

$$[\Delta\Phi_{i+1/2}]_{\text{posd}} = \text{sign}([\Delta\Phi_{i+1/2}]_{\text{avg}}) \times \min\{ |[\Delta\Phi_{i+1/2}]_{\text{avg}}|, 2\Phi_{i+1/2} \}. \quad (3b)$$

That is, by limiting the magnitude of the mismatch to be no greater than twice the mean value itself, positive definiteness of the distribution can be maintained. Equation (3b) together with the flux form transport equation (1) is the simplest positive-definite van Leer-type scheme that we know of. It contains the smallest possible implicit diffusion when and where it is needed

to make the linear subgrid distribution positive definite. If, in addition to a lower bound, a local upper bound  $\Phi_{i+1/2}^{\max}$  (e.g., the saturation mixing ratio for the water vapor) is desired, we set

$$\Delta\Phi_{i+1/2} = \text{sign}([\Delta\Phi_{i+1/2}]_{\text{avg}}) \min\{ |[\Delta\Phi_{i+1/2}]_{\text{avg}}|, 2 \text{ DIM}(\Phi_{i+1/2}, \Phi_{i+1/2}^{\min}), 2 \text{ DIM}(\Phi_{i+1/2}^{\max}, \Phi_{i+1/2}) \}. \quad (3c)$$

Equation (3c) together with (1a)–(1c) is a more general transport scheme than that originally given by van Leer (1977, 1979). The constraint in (3c) forces the distribution to be bounded by  $\Phi_{i+1/2}^{\min}$  and  $\Phi_{i+1/2}^{\max}$  (if initially so), which is similar to the concept of the flux limiters in the flux-corrected transport (FCT) of Boris and Book (1973) and Zalesak (1979). Since the limiter is applied to the mismatch, which is essentially a free parameter in this scheme, rather than the flux as in FCT, better phase characteristics are expected. However, the limiter (3c) does not yet guarantee monotonicity unless the upper and lower limits are properly chosen.

In his original series of papers, van Leer (1977, 1979) proposed several formulations of the mismatch (slope in his terminology) to ensure the upstream-biased transport represented by (1) to be monotonic. Among them, a very simple choice that yields true monotonicity while retaining second-order accuracy is the one applied by ADRG [cf. their Eq. (2.4)]:

$$[\Delta\Phi_{i+1/2}]_{\text{mono4}} = \begin{cases} \frac{\delta\Phi_i \delta\Phi_{i+1}}{[\Delta\Phi_{i+1/2}]_{\text{avg}}}, & \text{if } \text{sign}(\delta\Phi_i) = \text{sign}(\delta\Phi_{i+1}) \\ 0, & \text{otherwise.} \end{cases} \quad (4)$$

That is, instead of simply using the algebraic mean, the harmonic mean of the two one-sided differences is taken as the mismatch when  $\Phi_{i+1/2}$  is not a local extremum. ADRG have demonstrated that van Leer's scheme using (4) is sufficiently accurate for their ozone transport calculations when a  $2^\circ \times 2.5^\circ$  (latitude–longitude) grid resolution is used. It is, in fact, significantly better than the global spectral method at that resolution. However, we point out that the monotonicity constraint (4) is unnecessarily strong, particularly at low resolution. To further reduce the implicit diffusion of the scheme, the constraint on the mismatch must be relaxed as much as possible toward  $[\Delta\Phi_{i+1/2}]_{\text{avg}}$ . To this end, we return to the general form (3c) and make use of the following locally determined limiters:

$$\Phi_{i+1/2}^{\min} = \min\{\Phi_{(i-1)+1/2}, \Phi_{i+1/2}, \Phi_{(i+1)+1/2}\} \quad (5a)$$

$$\Phi_{i+1/2}^{\max} = \max\{\Phi_{(i-1)+1/2}, \Phi_{i+1/2}, \Phi_{(i+1)+1/2}\}. \quad (5b)$$

We deduce from (3c)

$$[\Delta\Phi_{i+1/2}]_{\text{mono5}} = \text{sign}([\Delta\Phi_{i+1/2}]_{\text{avg}}) \times \min\{ |[\Delta\Phi_{i+1/2}]_{\text{avg}}|, 2(\Phi_{i+1/2} - \Phi_{i+1/2}^{\min}), 2(\Phi_{i+1/2}^{\max} - \Phi_{i+1/2}) \}. \quad (5c)$$

The above constraint on the mismatch guarantees monotonicity by forcing the *subgrid distribution* to fall within the range spanned by the locally defined minimum (5a) and maximum (5b). It can be verified that this monotonic constraint is functionally equivalent to Eq. (66) of van Leer (1977). Since there is no need to check conditional flags (i.e., no "if" statements in the code) when computing the mismatches, it can be more efficiently vectorized on supercomputers than either (4) or van Leer's original form.

The implicit diffusion of the van Leer-type schemes discussed above is directly related to the magnitude of the mismatch (the steepness of the slope) of the subgrid linear distribution. The smaller the magnitude of the mismatch, the larger the implicit diffusion is. It is simple algebra to show that

$$|[\Delta\Phi_{i+1/2}]_{\text{avg}}| \geq |[\Delta\Phi_{i+1/2}]_{\text{posd}}| \geq |[\Delta\Phi_{i+1/2}]_{\text{mono5}}| \geq |[\Delta\Phi_{i+1/2}]_{\text{mono4}}|.$$

Although it is more diffusive than the positive-definite scheme (3b), van Leer's scheme that applies (5) is less diffusive than the one that applies (4), which was adopted by ADRG. Figure 3 shows the results of the transport of a rectangular wave of unit height in a 1D periodic domain after five revolutions (500 steps) using (3b), (4), and (5). Also included for comparison is the result using (3c) with the following fixed *global* limiters:

$$\Phi_{i+1/2}^{\min} = 0, \quad \Phi_{i+1/2}^{\max} = 1 \quad (\text{for all } i). \quad (6)$$

The superiority of van Leer's scheme using monotonic constraint (5) over (4) is clear. The positive-definite scheme (3b) overshoots, as could be expected. Although the transport using the fixed global constraint (6) gives the best result for this test, it is not strictly monotonic. It will produce local overshoots and undershoots in a more complicated configuration or when there are strong feedback mechanisms (e.g., source/sink terms). Nevertheless, the local overshoots/undershoots might be contained by the still present implicit diffusion. It is therefore possible that a scheme that applies only the fixed global limiters could be more accurate than that that applies a true monotonicity constraint such as (4) or (5). For example, for moisture transport, one can simply set the lower bound to zero globally and the upper bound to be the locally determined saturation density or other physically based value. As possibilities are numerous, in the preliminary study presented here, we will concentrate on the strictly monotonic constraint (5) and leave the exploration of other possibilities to the future. Finally, we note here

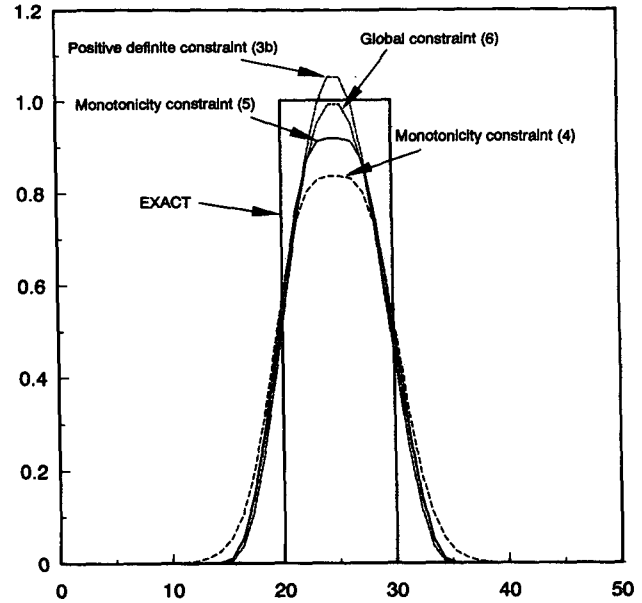


FIG. 3. The transport of a rectangular wave using the second-order van Leer-type scheme with four different constraints. The rectangular wave initially occupies 10 of the 50-cell periodic domain. The Courant number is 0.5 (500 steps).

that the fourth-order center difference scheme without a strong filter (i.e., diffusion) does not give a meaningful result in this test [not shown, but see Fig. 6 in Carpenter et al. (1990) for a comparison].

We now turn our attention to the implementation of the monotonic scheme to a  $\sigma$ -coordinate hydrostatic model on a sphere. The 3D flux form transport equation on a sphere can be written as

$$\frac{\partial}{\partial t} (\pi q) + \frac{\partial}{\partial x^*} (\pi q U) + \frac{1}{\cos\theta} \frac{\partial}{\partial y} (\pi q V \cos\theta) + \frac{\partial}{\partial \sigma} (\pi q \dot{\sigma}) + s = 0, \quad (7)$$

where  $x^* = a\lambda \cos\theta$ ,  $y = a\theta$ . The parameters  $q$ ,  $a$ ,  $\lambda$ ,  $\theta$ ,  $\pi$ , and  $s$  are the mixing ratio, earth's radius, longitude, latitude, surface pressure, and the source/sink term, respectively. Other symbols are standard. As mentioned previously, transport is done one spatial direction at a time using the prototype (1) and a suitable constraint on the mismatch. To conserve mass, it is important that the  $\pi$ -weighted mixing ratio ( $\pi q$ ) be the predicted quantity. Before transport,  $(\pi q)^n$  is computed as the direct product of  $\pi^n$  and  $q^n$ . After transport in all three dimensions is done, the mixing ratio is recovered as follows:

$$q^{n+1} = \frac{(\pi q)^{n+1}}{\pi^{n+1}}. \quad (8)$$

Total moisture will be conserved as long as total *air mass* is conserved (more about this in the next section).

The direct prediction of the mixing ratio in ADRG [their Eq. (2.5)] does not conserve mass unless the computation of the vertical velocity is modified to enforce mass conservation, which unfortunately would alter the model's dynamics, and is therefore not recommended for moisture transport in a GCM.

The time step  $\Delta t$  in an explicit global gridpoint model is primarily limited by the pressure gradient terms in the momentum equations. The constituent transport equation does not have such terms, and consequently, the time step can be much larger than that for other prognostic variables. In the tests presented in the following section, for simplicity, we chose the same time step for the moisture transport. Further time splitting in the zonal direction is still needed at high latitudes (poleward of  $80^\circ$  for a GCM using an explicit time integration scheme and a polar filter) to keep the local zonal Courant number less than unity. For a  $4^\circ \times 5^\circ$  resolution simulation using the GLA GCM, we need only to split the zonal transport at  $82^\circ$  and  $86^\circ$  into two and four substeps, respectively. (Note that zonal transport is not necessary inside polar caps.) The computation overhead caused by the converging meridians is therefore very small. Also, as the zonal resolution at  $86^\circ$  is extremely high (as compared to the meridional resolution), there is no noticeable loss of accuracy if we set the mismatches (in the zonal direction) there to be zero.

The computation of the fluxes into/out of polar caps is similar to that of ADRG except that mismatches inside polar caps *in the meridional direction* as viewed from different longitudes are explicitly calculated rather than simply set to zero. Take the northern polar cap for example, as illustrated in Fig. 4, the mismatch as viewed from longitude  $x_i^*$  is determined by  $\Phi_{i,np-1}$ ,  $\Phi_{i,np}$ , and  $\Phi_{iop,np-1}$ , where  $\Phi_{iop,np-1}$  is the value across the North Pole opposite to  $\Phi_{i,np-1}$ . We obtain from (5)

$$\Delta\Phi_{i,np} = \text{sign}([\Delta\Phi_{i,np}]_{\text{avg}}) \min\{ |[\Delta\Phi_{i,np}]_{\text{avg}}|, 2(\Phi_{i,np} - \Phi_{i,np}^{\min}), 2(\Phi_{i,np}^{\max} - \Phi_{i,np}) \},$$

where

$$\begin{aligned} \Phi_{i,np}^{\min} &= \min\{\Phi_{i,np}, \Phi_{i,np-1}, \Phi_{iop,np-1}\}, \\ \Phi_{i,np}^{\max} &= \max\{\Phi_{i,np}, \Phi_{i,np-1}, \Phi_{iop,np-1}\} \\ [\Delta\Phi_{i,np}]_{\text{avg}} &= \frac{1}{2}(\Phi_{iop,np-1} - \Phi_{i,np-1}). \end{aligned}$$

The mismatch as viewed from the other side of the polar cap has the same magnitude but with the opposite sign; that is,  $\Delta\Phi_{iop,np} = -\Delta\Phi_{i,np}$ . Finally, in the computation of the vertical transport, the top and the lowest layers can be assumed to be well mixed (i.e., vanishing mismatch), which is a good approximation from a physical standpoint. For water vapor transport, the mismatch in the top layer can be more accurately computed by adding a hypothetical dry layer above the top

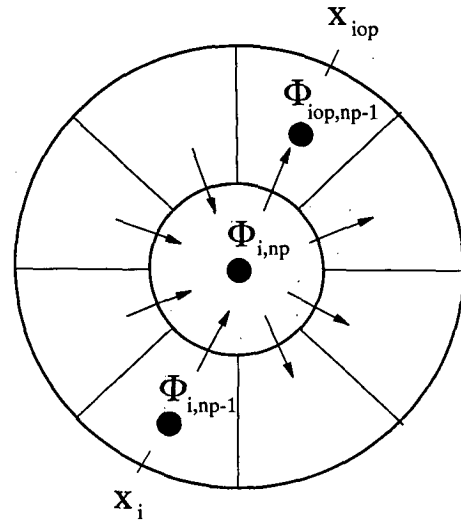


FIG. 4. Determination of the mismatches inside the northern polar cap.

constant pressure boundary, which is at 10 mb in the GLA GCM.

### 3. Comparisons with the fourth-order center-differencing scheme

We have performed two types of tests to compare the characteristics of our implementation of the second-order van Leer scheme on a sphere using the monotonicity constraint (5) (MVL2, hereafter) with that of the fourth-order center-differencing scheme (CD4, hereafter) currently used in the GLA GCM for the horizontal discretization of all prognostic variables. The first type of tests is the 2D (horizontal only) noninteractive shape-preserving transport, which, we believe, demonstrates the potential of the van Leer scheme. The second type of test is a summer climate simulation using the GLA GCM with full physics.

#### a. Noninteractive shape-preserving transports

Two different initial distributions (a cosine hill and a plateaulike distributions) are transported at two different resolutions,  $4^\circ \times 5^\circ$  and  $2^\circ \times 2.5^\circ$ , respectively, by a solid-body rotating wind field (axis of rotation is perpendicular to the axis of the earth's rotation) as given by Williamson and Rasch (1989). The cosine hill (Fig. 5a) represents a smooth distribution more typical of large-scale (and lower frequency) meteorological fields while the plateaulike distribution (Fig. 7a) resembles a front or a shock (a discontinuity in space or in time) in a less typical situation or when there are strong source or sink terms. Note that the  $4^\circ \times 5^\circ$  resolution is very low by today's standard, but it is still being used for long-term climate simulations, particularly in coupled ocean-atmosphere models. Al-

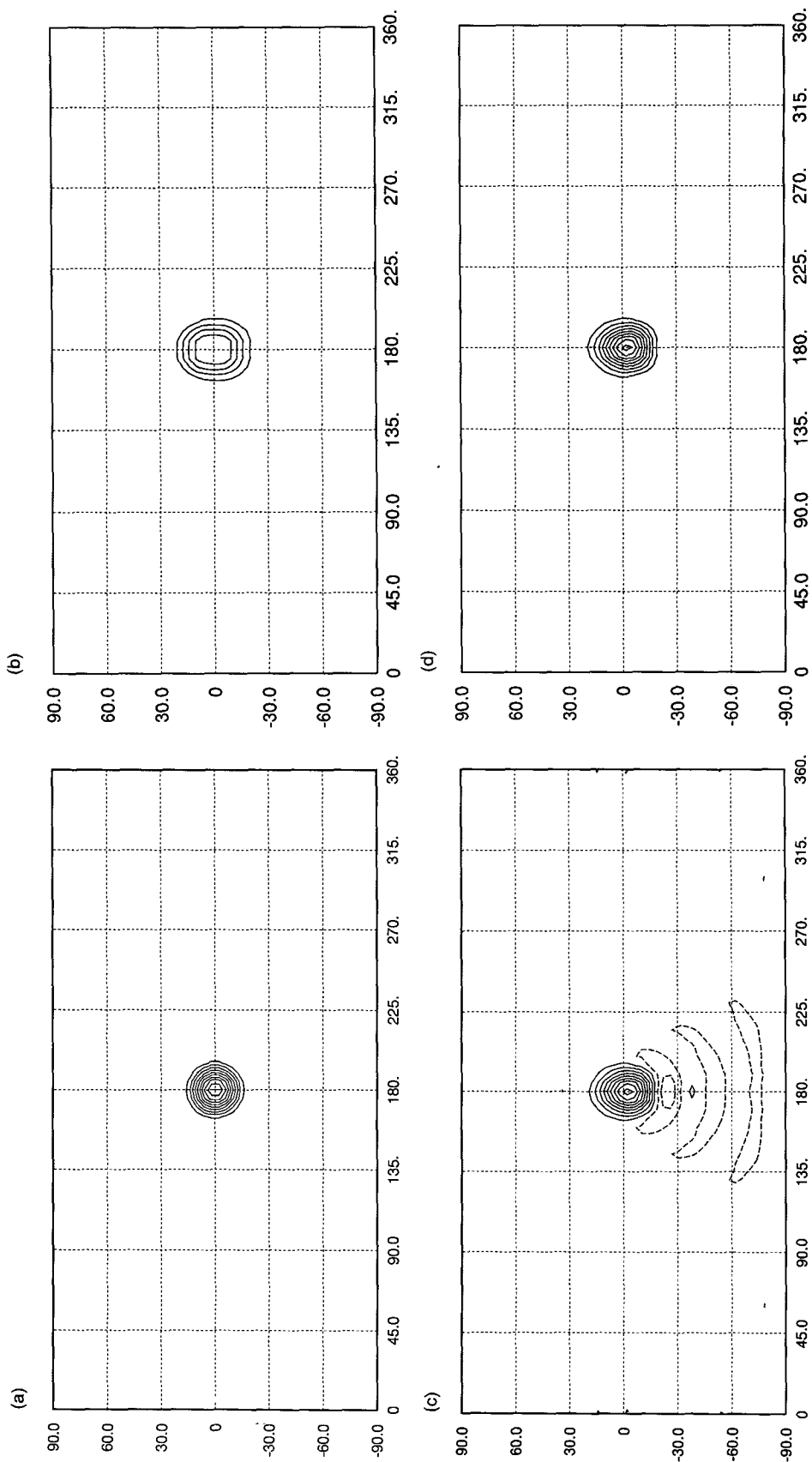


Fig. 5. Transport of the cosine hill by MVL2 and CD4 on the regular  $4^\circ \times 5^\circ$  grid. The original peak value is 1. The contour interval is 0.1 except that the 0 contour is replaced by the  $-0.01$  contour. Values smaller than  $-1.0 \times 10^{-4}$  are shaded: (a) the initial (exact) distribution; (b) MVL2 after one full revolution; (c) CD4 after one full revolution; and (d) CD4 after one full revolution but with negative values fixed.

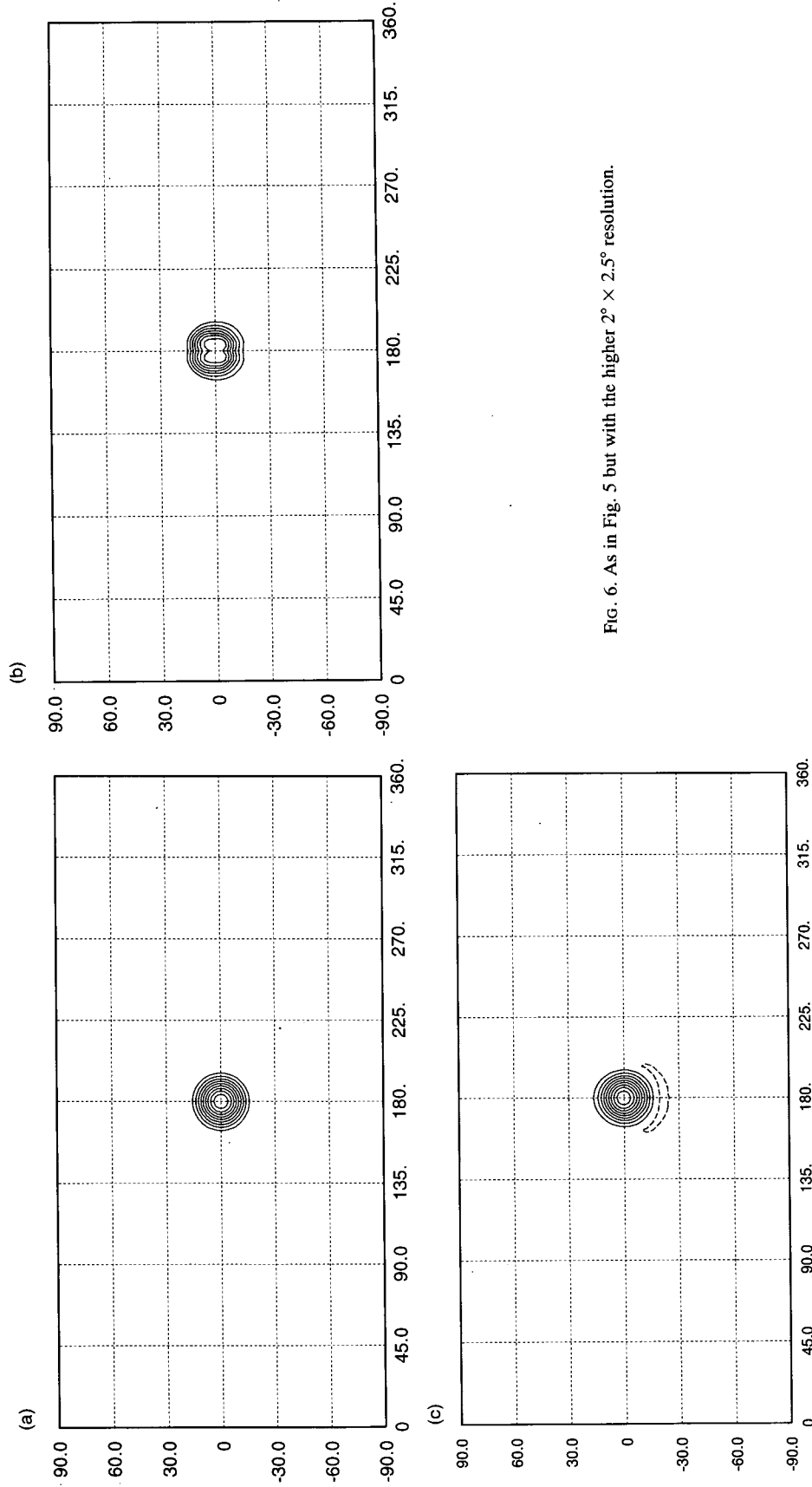


FIG. 6. As in Fig. 5 but with the higher  $2^\circ \times 2.5^\circ$  resolution.

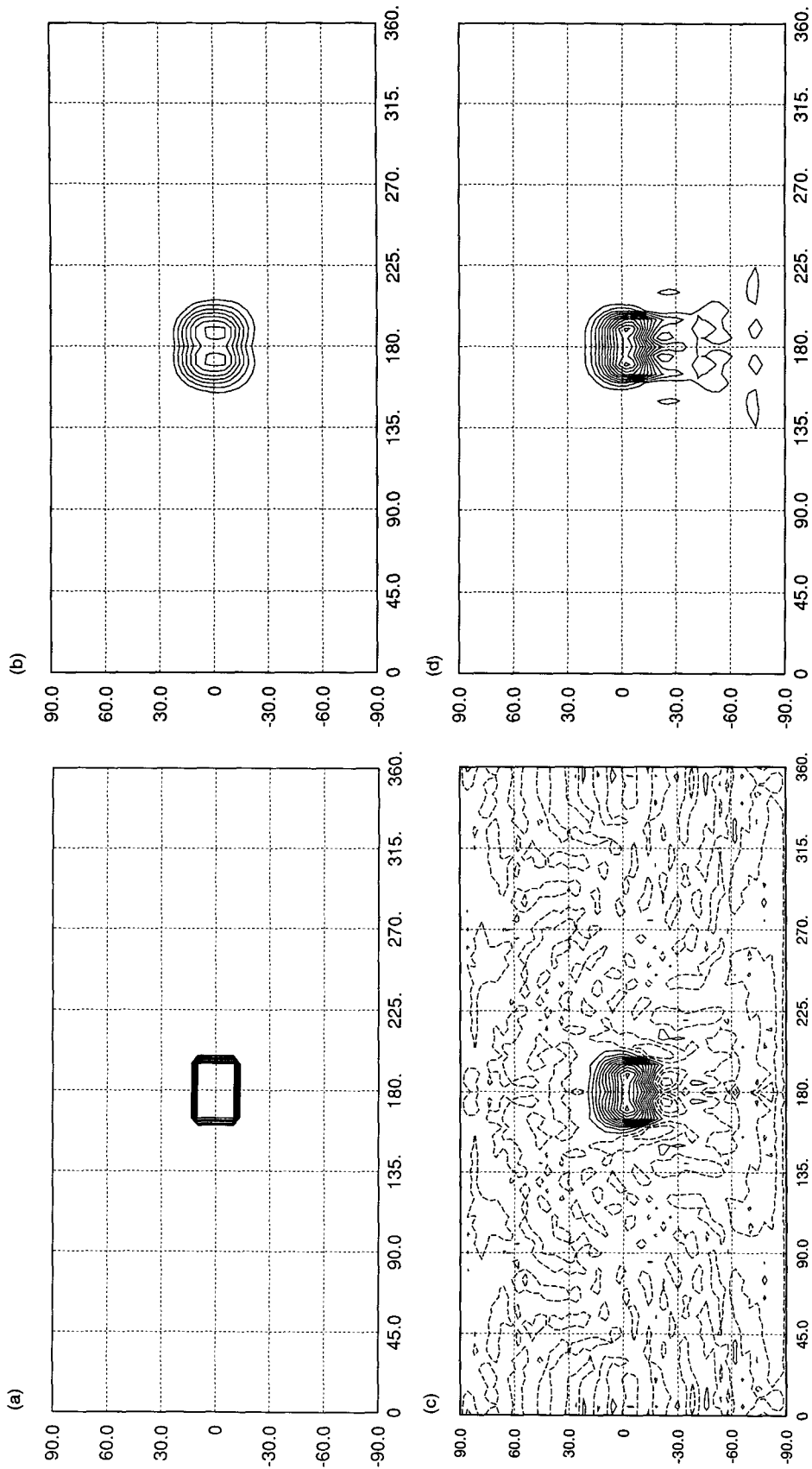


FIG. 7. As in Fig. 5 but for the plateaulike distribution.

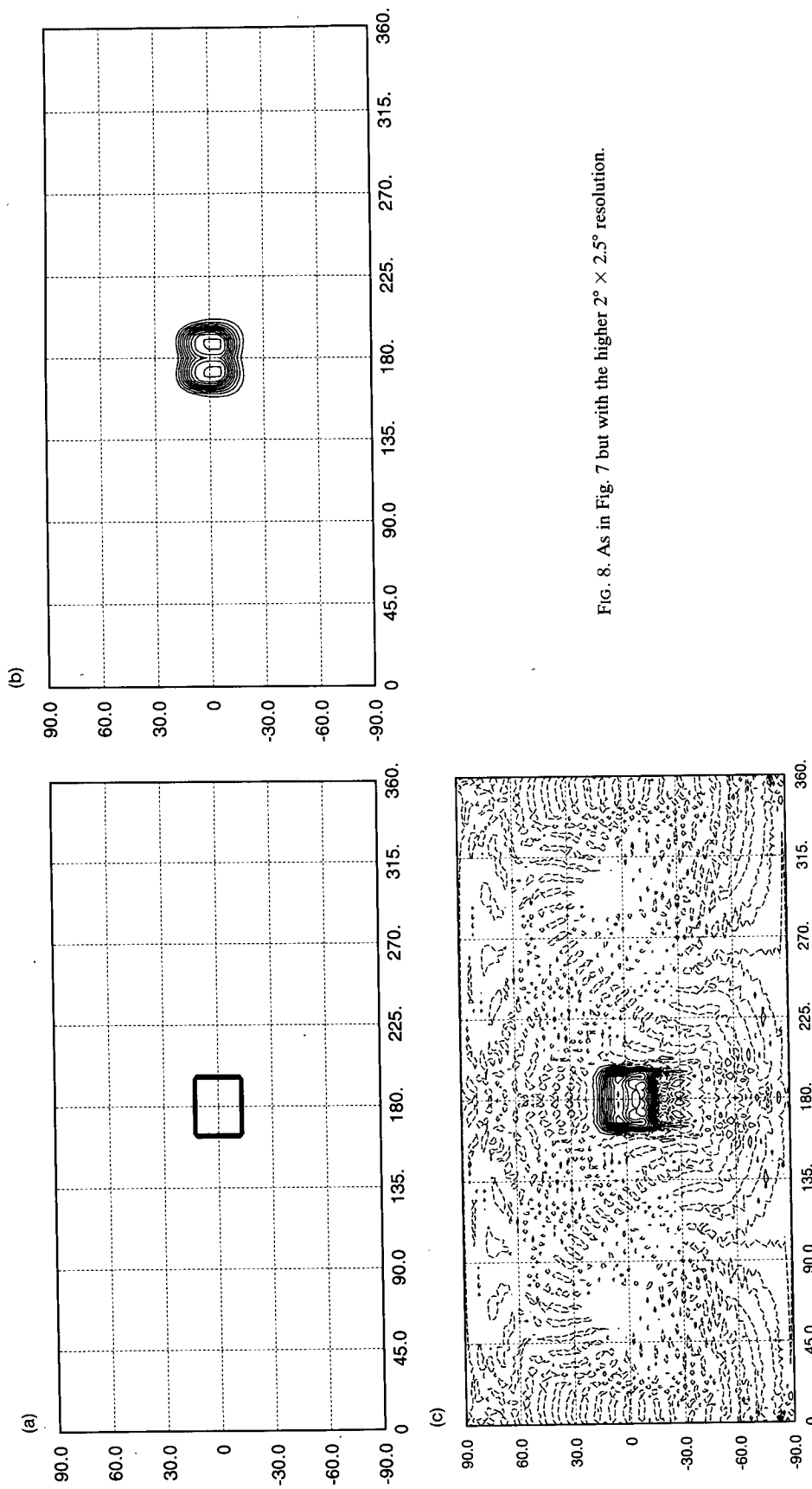


FIG. 8. As in Fig. 7 but with the higher  $2^\circ \times 2.5^\circ$  resolution.

TABLE 1. Particulars of the 17-layer GLA GCM.

No.	Item	Description	Reference
1	Horizontal resolution	4° lat × 5° long	Kalnay et al. (1983)
2	Vertical resolution	17 $\sigma$ layers	Fox-Rabinovitz et al. (1991)
3	Longwave radiation	Modified HV* radiation package	Harshvardhan et al. (1987)
	(a) Water vapor and CO <sub>2</sub> absorption	An adaptation of Chou and Chou-Peng	Chou (1984) Chou and Peng (1983)
	(b) Ozone absorption	Modified Rodgers	Rodger (1968) and Rosenfield et al. (1987)
4	Shortwave radiation	Slightly modified HV radiation package	Harshvardhan et al. (1987)
	(a) Ozone absorption, water vapor absorption, and Rayleigh scattering	Slightly modified Lacis and Hansen	Lacis and Hansen (1974)
	(b) Aerosol absorption and scattering	Sud and Walker using Pinker and Laszlo (1992)	Formulated by Harshvardhan**
5	Turbulence and PBL	Mellor-Yamada 2.5	Helfand and Labraga (1988)
6	Biosphere	Simple biosphere (SiB)	Sellers et al. (1986) Sud et al. (1990) Xue et al. (1991)
7	Nonprecipitating	Relative humidity dependent fractional clouds	Sud and Walker (1992) Slingo (1987)
8	Cumulus clouds	Detraining anvils	Sud and Walker (1992)
9	Moist convection	An adaptation of Arakawa-Schubert (1974)	Sud et al. (1991) with Tokioka et al. (1988)
10	Large-scale precipitation	Fractional cover	Sud and Walker (1990)
11	Cumulus downdrafts	An unsaturated convective downdraft scheme	Sud and Walker (1993)
12	Convection and large-scale rain evaporation	Kessler (1969) with Ruprecht and Gray (1976) cloud fractions	Sud and Molod (1988)
13	Soil temperature parameterization	Force restore two layers	Deardoff (1987)
14	Soil moisture initialization and parameterization	Three soil layers initialization with off-line SiB	Sellers et al. (1986)
15	Vegetation properties roughness and biometry	Surface albedo analysis of vegetation data characteristics data	Dorman and Sellers (1989) ERBE data over bare land
16	General modification	Several improvements in the physics package	Sud and Walker (1990, for a detailed discussion)

\* HV—Harshvardhan.

\*\* Personal communication.

though a much larger time step can be used for both schemes, the time step used in the following tests is chosen to be consistent with that used in the full GCM simulations.

Figures 5b and 5c show the cosine hill distribution at the 4° × 5° resolution after one full revolution using MVL2 and CD4, respectively. As in the GLA GCM, the transport using CD4 uses a global 16th-order Shapiro filter and a polar Fourier filter, but no filling scheme is applied to fix the negative values the scheme generated. The Asselin time filter is also used as required by the leapfrog time integration scheme. Transport using MVL2, on the other hand, does not need any filtering in time or in space. A total of 900 time steps are used in both cases. Although it is evident that MVL2 is diffusive (only 49% of the peak amplitude is maintained), the overall shape of the distribution is predicted very well and there is essentially no phase error. The transport using CD4 maintains 95% of the

peak amplitude, which is much better than MVL2, but it overshoots initially, which helps to maintain the final peak value. Undershoots are present in the transport by CD4 for all time. The largest negative value generated at the end is 17% of the original (positive) peak value, and the spurious upstream wakes almost occupy the whole globe, despite the use of the highly scale-selective Shapiro filter. Figure 5d shows the same transport by CD4 [as in (5c)] but negative values are set to zero at the end of each time step. This is similar, as viewed horizontally, to the filling algorithm currently used in the GLA GCM in which mass is “borrowed” vertically from below to fix negative values. It is observed that the dispersive error is suppressed. But the phase error still exists, and the total mass is increased by 22%, which might be regarded as unacceptable. In the GCM simulations, the tactic of borrowing moisture from below is thus like having an artificial convection sending moisture upward and then dispersed horizontally re-

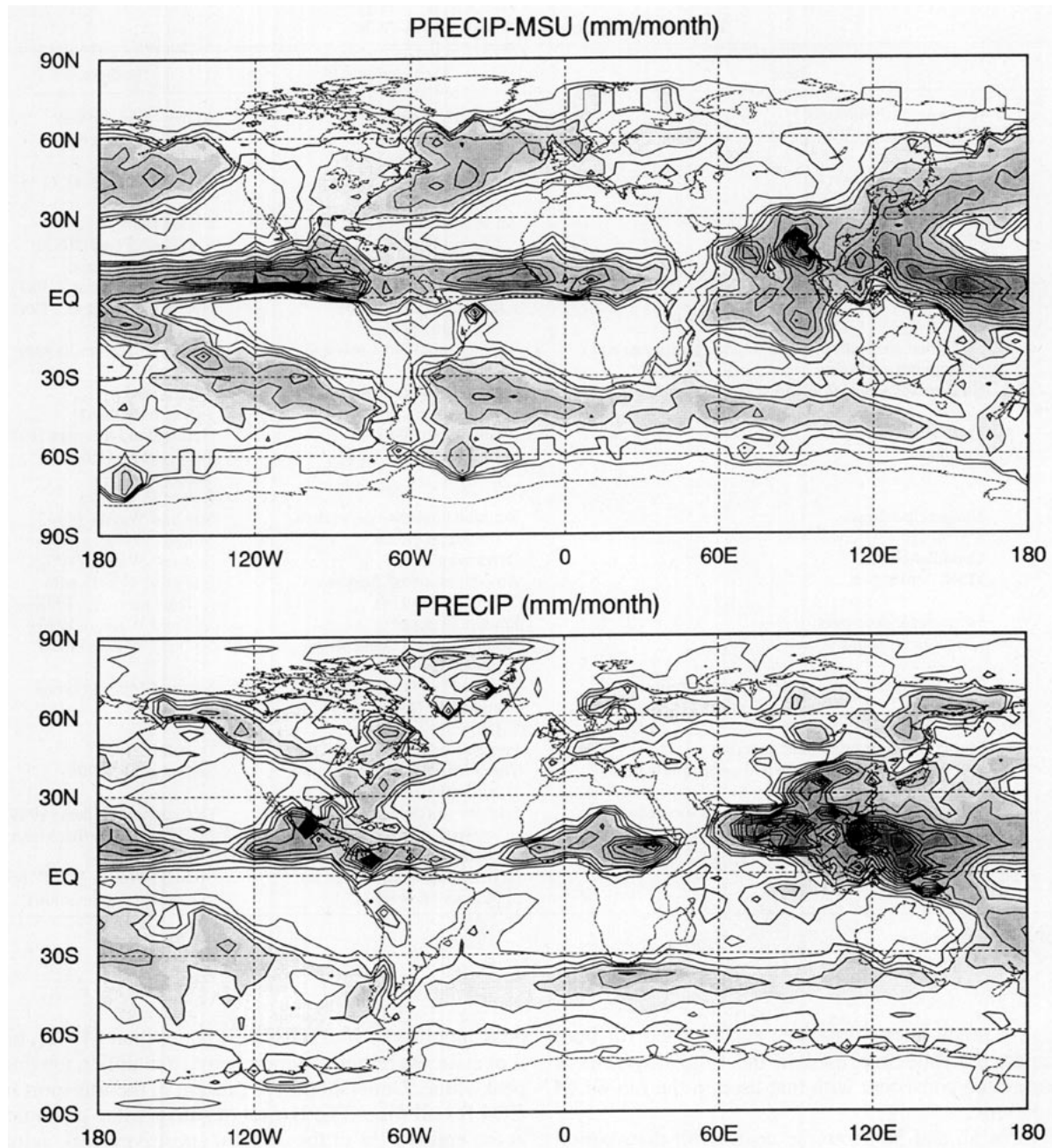


FIG. 9. Time mean precipitation ( $\text{mm month}^{-1}$ ) during summer 1987 from (a) the observations (MSU data over ocean and station data over land), (b) the control experiment, and (c) the MVL2 experiment. The contour interval is  $30 \text{ mm month}^{-1}$  for precipitation less or equal to 120; 60 otherwise. The darker shaded area has higher value.

ardless of the local vertical thermodynamic profile. This is perhaps justifiable if it is the vertical transport that creates the negative mixing ratio. The local predictability of the moisture field is lost, however, if the negative values are created by the horizontal transport, as in this test.

Figures 6a–c are the same as Figs. 5a–c but with the higher  $2^\circ \times 2.5^\circ$  resolution. The transport by CD4 (Fig. 5c) now uses an eighth-order Shapiro filter, as in

the GLA GCM for that resolution. A total of 1800 time steps are used. Both schemes have improved significantly, especially that of MVL2. The dispersive error of the CD4 is now less severe but still evident.

The cosine hill transport experiment does not exhibit a monotonic scheme's ability to handle sharp gradients or discontinuities. Figures 7a–d are the same as Figs. 5a–d but for a plateaulike distribution. Although the extreme disparity in resolution in the two spatial direc-

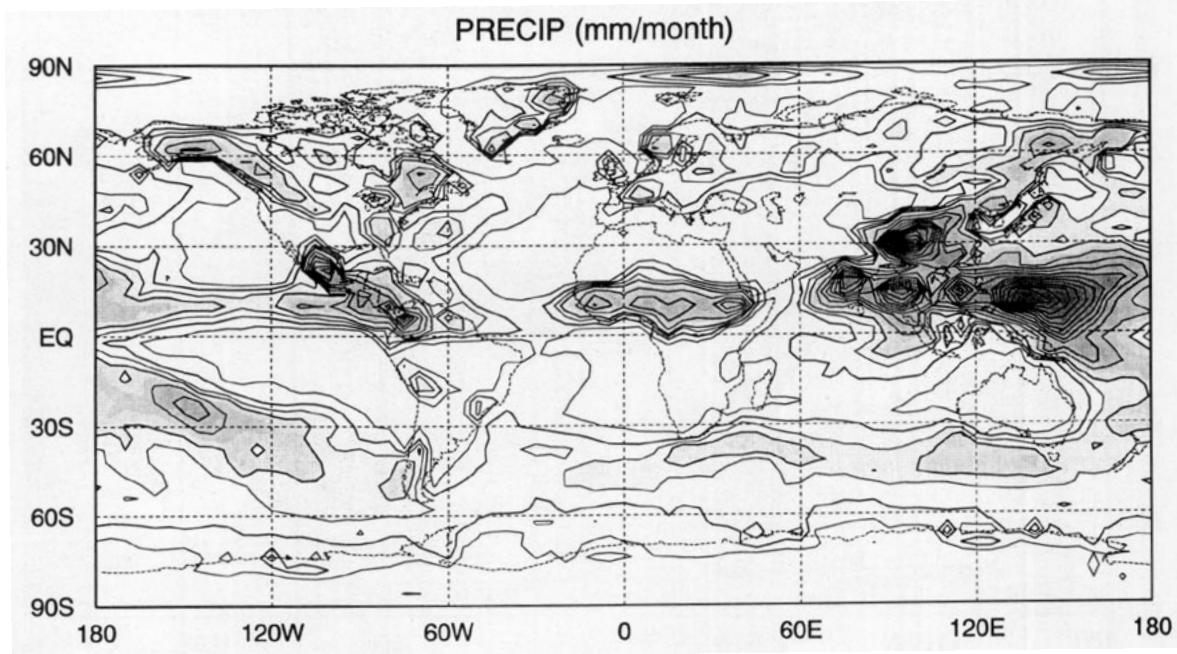


FIG. 9. (Continues)

tions near poles results in the formation of the double extrema,<sup>1</sup> the distribution is predicted quite well by MVL2 (Fig. 7b). The result by CD4 (Fig. 7c) has unacceptably large under- and overshoots and dispersive errors, even after negative values are fixed (Fig. 7d). Figures 8a–c show the transports at the higher  $2^\circ \times 2.5^\circ$  resolution. Again, the transport by MVL2 has improved significantly. The spurious oscillations generated by CD4 are still severe. The increase of resolution does not greatly improve the transport by CD4 in this case. This is a good case against the argument that low-order upwind-biased schemes are inferior. If the order of accuracy is the only criterion, then the global spectral method that has the highest possible order of accuracy is the best choice. Due to its global nature and the presence of the Gibbs phenomenon, we expect the spectral method to do even worse than CD4 in this particular test. As the resolution of global models is increasing with the ever increasing computer power, this problem would become more evident as smaller-scale structures as well as the irregular terrain of the earth can be better resolved.

The formal order of accuracy of a particular scheme can be misleading. First, all schemes reduce to first-order accuracy in the vicinity of discontinuities (in space or in time). Second, the time-filtered leapfrog scheme used by almost all global models is only first-

order-accurate in time, and the error is proportional to  $2\Delta t$ —not  $\Delta t$  as in a forward-in-time scheme such as the one proposed here. Likewise, spatial filtering also degrades the formal accuracy of the original scheme. For example, if one is to apply a Smagorinsky-type nonlinear friction (Smagorinsky 1963) to a spectral model, the model would formally become only second-order accurate in space. (Smagorinsky's nonlinear diffusion or the Shapiro filter widely used in gridpoint models introduces second-order truncation error in space.)

Since a Shapiro filter, a polar filter, a time filter, and a filling algorithm are needed with the transport by CD4 (or any other center-in-time and center-in-space differencing scheme), the total floating point operations required are greater than that of MVL2. In addition, the permanent memory usage of MVL2 is, at most, half of that required by CD4. It should also be noted here that since both the Shapiro filter and the time filter apply directly to the mixing ratio (or specific humidity in the case of moisture transport), mass is not exactly conserved by the transport using CD4.

#### b. GCM simulations

Two parallel three-month runs of the 17-layer A-grid GLA GCM with the full physics (see Table 1 for details) were carried out. The horizontal resolution used is  $4^\circ \times 5^\circ$ . The model is initialized with the data from the ECMWF analysis at 0000 UTC 1 June 1987. The first simulation designated as the “control” used the original CD4 code in the horizontal and a second-order center-differencing scheme in the vertical. The second simulation designated as “MVL2” used the identical

<sup>1</sup> It should be noted here that the analytically nondivergent wind has relatively large divergence near poles in its discretized form, which contributed to the formation of the double extrema.

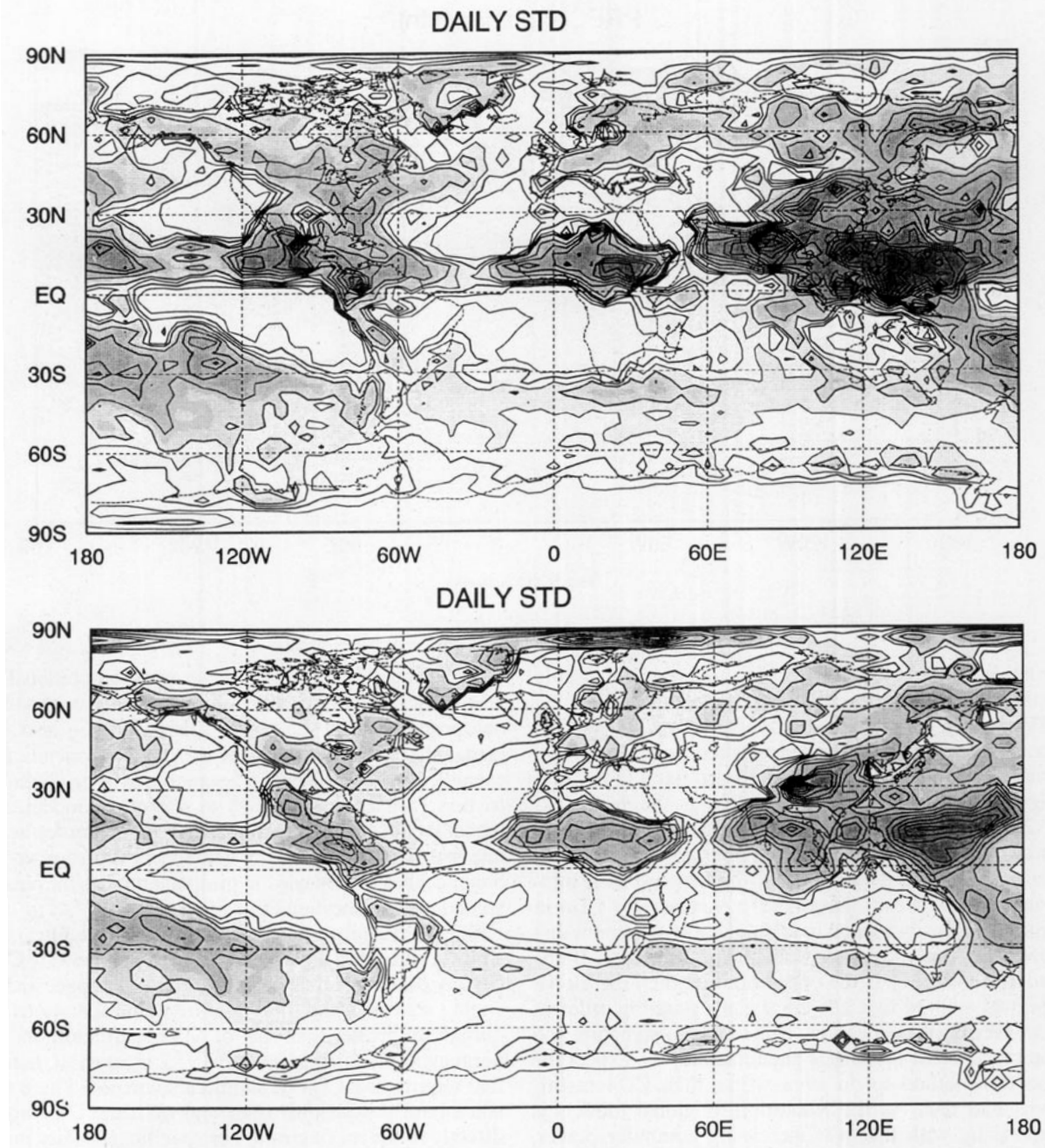


FIG. 10. The daily standard deviation precipitation from the seasonal mean for (a) the control experiment and (b) the MVL2 experiment. The contour interval is  $30 \text{ mm month}^{-1}$  for precipitation less or equal to 120; 60 otherwise. The darker shaded area has higher value.

code except that moisture transport has been replaced by the monotonic scheme represented by (1) and (5), as described previously.

The MVL2 scheme, by design, is a natural fit to a C-grid arrangement, but the A-grid version of the GCM was chosen owing to its more complete physics packages. Spatial averaging of the horizontal winds is there-

fore necessary for the moisture transport by MVL2. Note that spatial averaging is not needed for the vertical velocity, as it is already staggered with respect to the moisture field. For the moisture transport by MVL2, a straightforward second-order space-time average of the horizontal winds is taken at the end of the dynamic time step as follows:

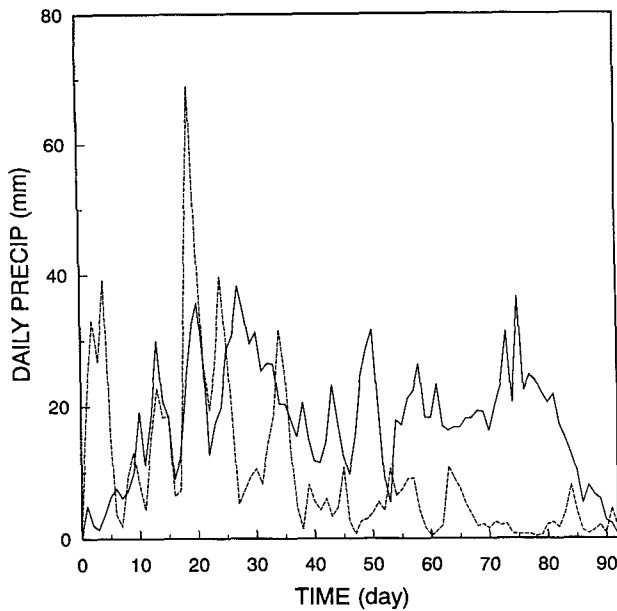


FIG. 11. The daily precipitation (mm) averaged along 6°N from 140° to 160°E. Solid line: the VL2 experiment. Dashed line: the control experiment.

$$\bar{U}_{i+1/2,j} = \frac{1}{4} (U_{i,j}^n + U_{i+1,j}^n + U_{i,j}^{n+1} + U_{i+1,j}^{n+1}),$$

$$\bar{V}_{i,j+1/2} = \frac{1}{4} (V_{i,j}^n + V_{i,j+1}^n + V_{i,j}^{n+1} + V_{i,j+1}^{n+1}).$$

The reason for using the time-averaged horizontal winds is to obtain better accuracy in time.

Since total air mass, which is proportional to the global mean surface pressure, is not exactly conserved when the time-filtered leapfrog scheme is used, exact moisture conservation is not possible. Fortunately, the degree of nonconservation of the total air mass is extremely small. The GLA GCM also has a routine that can be called to adjust the surface pressure to ensure the conservation of the total air mass. For computational efficiency, we chose the leapfrog scheme (with the Asselin time filter) for both experiments. We did carry out other short-term integrations using the Matsuno scheme to verify the exact conservation (excluding rounding error) of the moisture by MVL2.

Figures 9a, 9b, and 9c show the seasonal mean (summer 1987) precipitation from the observations,<sup>2</sup> the control experiment, and the MVL2 experiment, respectively. The MSU data has deficiencies at high latitudes due to erroneous or missing data points, we have filled

in the gap by a bilinear interpolation. A quality control is also performed to remove some isolated excessive values found in some subtropical regions over land. Due to these shortcomings and the model's limited predictability, we will not attempt to compare the numerical value grid points to grid points. Rather, it is the pattern that we shall emphasize.

It is clear that the precipitation from the MVL2 experiment is more closely correlated to the observations. Most notably, the South Pacific convergence zone (SPCZ), central Africa, the western Pacific, India, and Australia are regions where the MVL2 shows better structures over the control. Specifically, the SPCZ and the western Pacific convective regions in the MVL2 experiment are more coherently organized, as contrasted to the noisier control experiment. The Australia and Sahara deserts are also drier, and the rain distribution over central Africa is more in line with the observations. Note that both the control and MVL2 produced similar results in the Northern Hemispheric storm track regions.

There are a couple of places where the control is better than the MVL2. Namely, the MVL2 experiment produces too much large-scale precipitation near the North Pole (between 0° and 60°E) and less convective rainfall in the intertropical convergence zone (ITCZ) over the Atlantic Ocean. The reason, however, is not very clear. But the total area of these regions is relatively small. Considering the model's complexity and the less than perfect physics packages, it may or may not be directly related to the MVL2 scheme's known weakness—namely, its substantial implicit diffusion. In fact, as it is unfiltered, the zonal transport near the poles by MVL2 is far more accurate than that by CD4. Since the potential temperature advection is unmodified, the abnormal precipitation near the North Pole in the MVL2 run could possibly be caused by the spurious oscillations in potential temperature alone.<sup>3</sup>

A noteworthy improvement of the MVL2 experiment is that the excessive instantaneous precipitation rate occasionally found in the control is substantially reduced or completely eliminated. As the precipitation produced by MVL2 is more coherently organized both in space and time, the maximum time mean precipitation of MVL2 as shown in Fig. 9c is actually higher than that of the control shown in Fig. 9b (938 mm month<sup>-1</sup> versus 882 mm month<sup>-1</sup>). Figures 10a,b show the standard deviation of the daily precipitation from the time mean. Note that the standard deviation of the control is significantly higher than that of MVL2. Again, the pattern of MVL2 is less noisy and better organized than the control. The maximum value is 839

<sup>2</sup> The observations are the combination of the Microwave Sounding Unit (MSU) data over ocean (Spencer 1993) and the station data over land (Schemm et al. 1992).

<sup>3</sup> It is our conjecture that, in the control run, the spurious oscillations of the temperature and water vapor are in phase, and therefore, they caused less large-scale condensation near the North Pole than that in the MVL2 run.

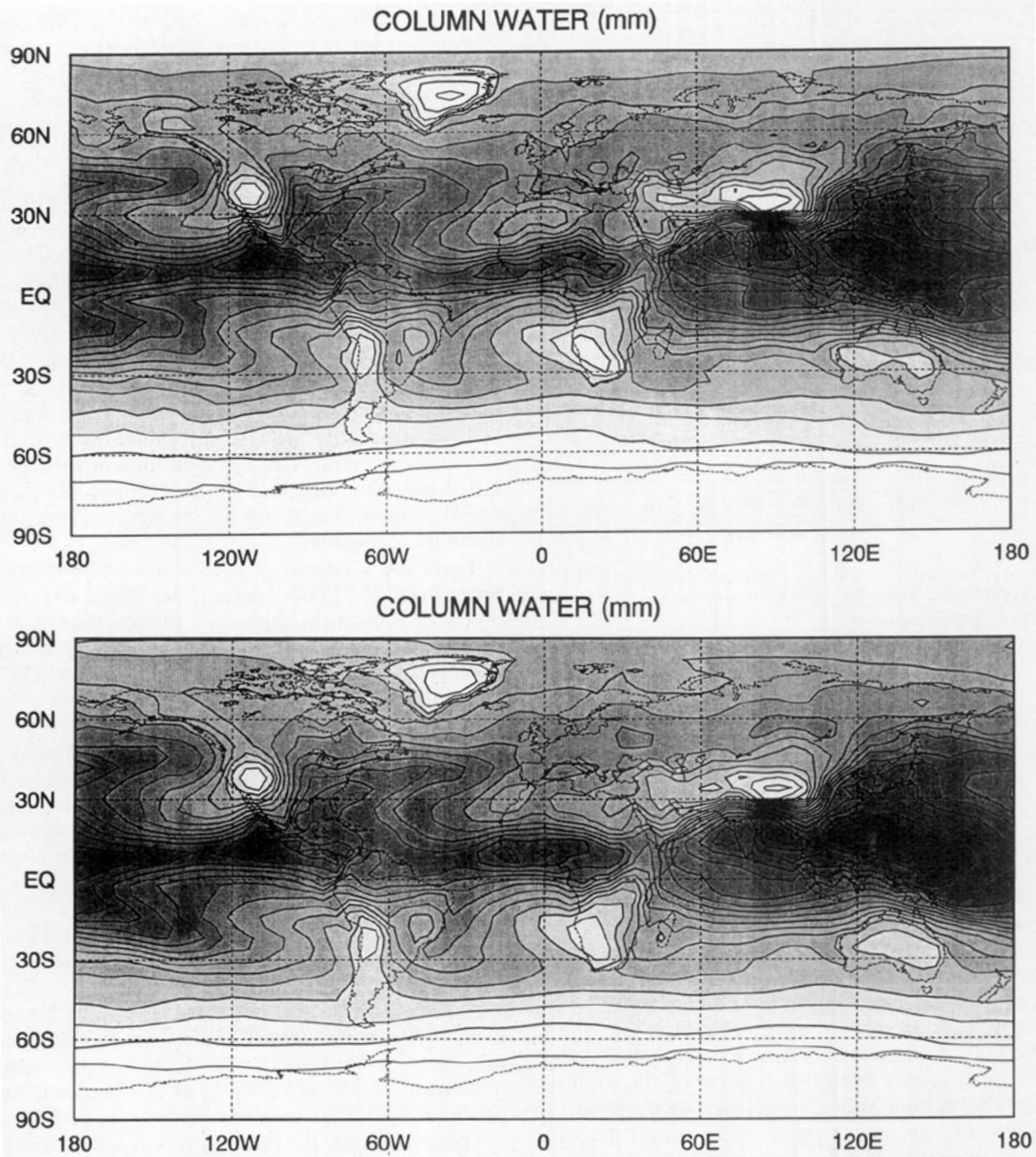


FIG. 12. The time mean column precipitable water predicted by (a) the control experiment and (b) the MVL2 experiment. The contour interval is 5 mm. The darker shaded area has higher value.

mm month<sup>-1</sup> for the control versus 777 mm month<sup>-1</sup> for the MVL2 experiment. The global means are 137 mm month<sup>-1</sup> and 103 mm month<sup>-1</sup> for the control and MVL2, respectively. To further illustrate this point, the accumulated daily precipitation averaged along 6°N from 140° to 160°E produced by these two experiments are compared in Fig. 11. It is noted that the control run initially produced substantially higher precipitation than that of MVL2. After following different paths of

initial adjustment, these two curves are in phase from day 7 to about day 25 and then become completely uncorrelated after that. Note that the control run produced an excessive precipitation of about 70 mm on day 20. (Keep in mind that this is the value averaged over a large 4° × 20° area in the Tropics.)

Figures 12a and 12b show the time mean column precipitable water predicted by the control and MVL2, respectively. Unlike the precipitation field,

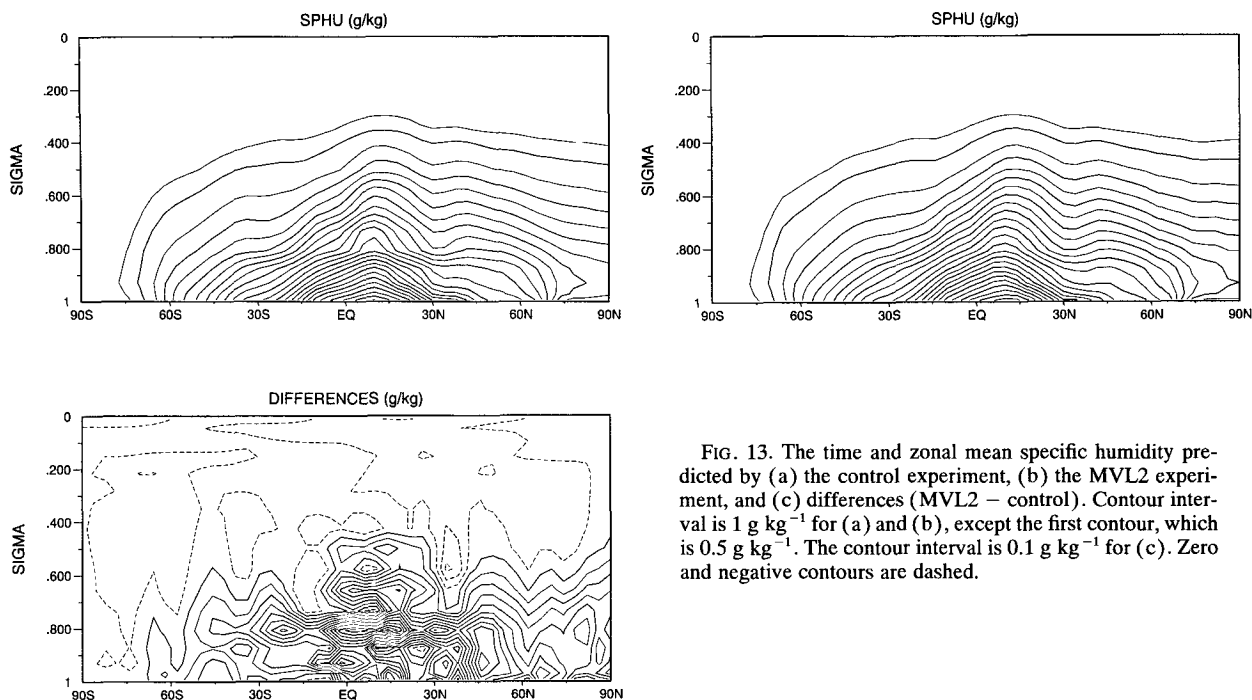


FIG. 13. The time and zonal mean specific humidity predicted by (a) the control experiment, (b) the MVL2 experiment, and (c) differences (MVL2 - control). Contour interval is  $1 \text{ g kg}^{-1}$  for (a) and (b), except the first contour, which is  $0.5 \text{ g kg}^{-1}$ . The contour interval is  $0.1 \text{ g kg}^{-1}$  for (c). Zero and negative contours are dashed.

which is sensitive to the transients of the moisture and therefore highly dependent on the transport scheme, the *time mean* column precipitable water fields are, to a large extent, controlled by the boundary forcing (i.e., surface fluxes and topography) and less by the exact manner moisture is transported. As a result, these two plots are quite similar. Nevertheless, we can still observe some differences between these two. For example, the atmosphere over the Australia and Sahara deserts is drier in the MVL2 experiment, and the moisture distribution of these two runs over the western Pacific convective region are quite different. Figures 13a, 13b, and 13c show the vertical cross sections of the zonal mean specific humidity of the control (CD4), MVL2 experiments, and their differences (MVL2 - CD4), respectively. The atmosphere in the MVL2 experiment is moister in the tropical lower troposphere (by as much as  $1.3 \text{ g kg}^{-1}$ ) but is slightly drier in the upper troposphere. The global mean precipitable water predicted by the control and the MVL2 experiments are 37 and 38.6 mm, respectively. Both experiments overestimated the total precipitable water by roughly 50% (assuming the observed value is 25 mm). Rasch and Williamson (1991) using a T42 spectral model with 12 vertical layers simulated a 20% drier atmosphere. While the T42 spectral model has much better equivalent horizontal resolution (particularly in the tropics) than our  $4^\circ \times 5^\circ$  regular grid resolution, we believe it is primarily the model physics that makes the difference. This problem is currently being studied.

#### 4. Summary and concluding remarks

We have derived a general form of a van Leer-type transport scheme. The constraint (3c) is very general. A simple positive-definite scheme can be obtained by setting the lower limit to zero and by not placing an upper limit. By choosing an appropriate set of global limiters (thus the *local* monotonicity is not guaranteed), it is possible to obtain a very simple yet accurate upstream-biased scheme with minimal implicit diffusion. For moisture transport, a physically motivated choice would be the locally defined saturation density as the upper bound and zero as the lower bound. Our present choice, however, is the truly monotonic scheme using the locally defined constraint (5). It is argued that in a highly nonlinear flow field or when there are strong source/sink terms, a transport scheme that guarantees absolute local monotonicity should be a better choice, despite its stronger implicit diffusion.

We have compared the original finite-difference scheme for moisture transport with the monotonic MVL2 scheme in the A-grid GLA GCM. Evidently, the improvements in the precipitation field are substantial. Several major problems associated with the traditional finite-difference schemes are solved or eased by the use of the monotonic scheme: namely, the false generation of the negative mixing ratio, the numerically produced supersaturation, and the uncertainty in the choice of suitable damping schemes (and their associated free parameters). In a  $\sigma$ -coordinate model, the usual tactic of "horizontal" filtering along

the constant  $\sigma$  surface is, to say the least, problematic near steep mountains. With the monotonic constraint on its implied subgrid distribution, the monotonic scheme reported here does not need any sort of "subgrid-scale turbulence parameterizations" or filtering. In fact, the MVL2 scheme, with the local monotonicity constraint on its implied subgrid distribution, can be regarded as a second-order finite-difference scheme with a near-optimal built-in subgrid-scale parameterization. In the GCM simulation with MVL2 scheme, the interior vertical diffusion on the moisture field is not removed, because it is an integral part of the moisture fluxes from the surface and cannot be easily separated.

We note that the MVL2 scheme presented here is free of the Gibbs phenomenon. As demonstrated by the transport of the plateaulike distribution, the accuracy of the MVL2 scheme will keep increasing with increasing resolution even when discontinuities or steep gradients are encountered. This is not so with traditional center-differencing schemes or spectral methods, whose accuracy could actually deteriorate if the sharp gradients can be better resolved by the increased resolution. Due to this shock handling ability, the monotonic scheme is well suited for short-term weather prediction and/or data assimilation where raw data from observations are constantly injected.

Finally, we note that the time and directional splitting formulation adopted here is an attractive alternative to the semi-Lagrangian approach to overcome the severe time-step restriction associated with the poles. Unlike traditional monotonic semi-Lagrangian schemes, mass (barring from rounding error) is exactly conserved by the van Leer-type schemes. One weakness that we are aware of with the second-order monotonic scheme (MVL2) is its substantial implicit diffusion at low resolution. The implicit diffusion can be reduced by further relaxing the monotonic constraint. For example, instead of the truly monotonic local constraint, one could use a global constraint or the positive-definite constraint [Eq. (3b)]. If that is still not satisfactory, a higher-order version of the scheme [e.g., the more expensive PPM, Colella and Woodward (1984)] can be used under the same general framework as presented in this paper. We recommend that forward-in-time dissipative monotonic schemes, or at the very least, positive-definite schemes, be preferred over the nondissipative but dispersive center-in-time and center-in-space schemes for transport of scalars in GCMs, particularly at high resolution.

*Acknowledgments.* We thank Dr. K.-M. Lau for his moral support in launching the project that supported this work. Financial support from NASA Earth Science and Applications Division as part of NASA participation in the TOGA COARE program was indispensable.

## REFERENCES

- Arakawa, A., and W. H. Schubert, 1974: Interaction of cumulus cloud ensemble with the large-scale environment. Part I. *J. Atmos. Sci.*, **31**, 674–701.
- Allen, D. J., A. R. Douglass, R. B. Rood, and P. D. Guthrie, 1991: Application of a monotonic upstream-biased transport scheme to three-dimensional constituent transport calculations. *Mon. Wea. Rev.*, **119**, 2456–2464.
- Boris, J. P., and D. L. Book, 1973: Flux-corrected transport. I: SHASTA, a fluid transport algorithm that works. *J. Comput. Phys.*, **18**, 38–69.
- Carpenter, R. L., Jr., K. K. Droegemeier, P. R. Woodward, and C. E. Hane, 1990: Application of the piecewise parabolic method to meteorological modeling. *Mon. Wea. Rev.*, **118**, 586–612.
- Chou, M.-D., 1984: Broadband water vapor transmission function for IR flux computations. *J. Atmos. Sci.*, **41**, 1775–1778.
- , L. Peng, and A. Arking, 1983: A parameterization of absorption in the 15 mm CO<sub>2</sub> spectral region with application to climate sensitivity studies. *J. Atmos. Sci.*, **40**, 2183–2192.
- Colella, P., and P. R. Woodward, 1984: The piecewise parabolic method (PPM) for gas-dynamical simulations. *J. Comput. Phys.*, **54**, 174–201.
- Deardorff, J. W., 1987: Efficient prediction of ground surface temperature and moisture with inclusion of a layer of vegetation. *J. Geophys. Res.*, **83**, 1889–1903.
- Doorman, J. L., and P. J. Sellers, 1989: A global climatology of albedo, roughness length, and stomatal resistance for atmospheric general circulation models as represented by simple biosphere model (SiB). *J. Appl. Meteor.*, **28**, 833–855.
- Fox-Rabinovitz, M., H. M. Helfand, A. Hou, L. L. Tackas, and A. Molod, 1991: Numerical experiments on forecasting climate simulation and data assimilation with the new 17 layer GLA GCM. *Ninth Numerical Weather Prediction Conf.*, Denver, CO, Amer. Meteor. Soc. 506–509.
- Harshvardhan, R. Davis, D. A. Randall, and T. G. Corsetti, 1987: A fast radiation parameterization for general circulation models. *J. Geophys. Res.*, **92**, 1009–1016.
- Helfand, H. M., and J. C. Lebraga, 1988: Design of a non-singular level 2.5 second order closure model for prediction of atmospheric turbulence. *J. Atmos. Sci.*, **45**, 113–132.
- Kalnay, E., R. Balgovic, W. Chao, D. Edlmann, J. Pfendner, L. Takacs, and K. Takano, 1983: Documentation of the GLAS fourth order general circulation model. Volume I. NASA Tech. Memo. 86064, NASA Goddard Space Flight Center, Greenbelt, MD.
- Kessler, E., 1969: On the distribution and continuity of water substance in the atmospheric circulation. *Meteor. Monogr.*, No. 32, Amer. Meteor. Soc., 1–84.
- Lacis, A., and J. E. Hansen, 1974: A parameterization for the absorption of solar radiation in the earth's atmosphere. *J. Atmos. Sci.*, **31**, 118–133.
- Pinker, R. T., and I. Laszlo, 1992: Global distribution of photosynthetically active radiation as observed from satellites. *J. Climate*, **5**, 56–65.
- Rasch, P. J., and D. L. Williamson, 1991: The sensitivity of a general circulation model climate to the moisture transport formulation. *J. Geophys. Res.*, **96**, 13 123–13 137.
- Rodgers, C. D., 1968: Some extension and application of new random model for molecular and band frequency. *Quart. J. Roy. Meteor. Soc.*, **94**, 99–102.
- Rosenfield, J. E., M. R. Schoeberl, and M. A. Geller, 1987: A computation of the stratospheric diabatic circulation using an accurate radiative transfer model. *J. Atmos. Sci.*, **44**, 859–876.
- Ruprecht, E., and W. M. Gray, 1976: Analysis of satellite-observed tropical cloud clusters. II: Thermal, moisture and precipitation fields. *Tellus*, **28**, 414–426.
- Schemm, J., S. Schubert, J. Terry, and S. Bloom, 1992: Estimates of monthly mean soil moisture for 1979–1989. NASA Tech. Memo. 104571, 260 pp.

- Sellers, P. J., Y. Mintz, Y. C. Sud, and A. Dalcher, 1986: A simple biosphere model (SiB) for use within general circulation models. *J. Atmos. Sci.*, **43**, 505–531.
- Slingo, J., 1987: The development and verification of a cloud prediction scheme for the ECMWF model. *Quart. J. Roy. Meteor. Soc.*, **106**, 747–770.
- Smagorinsky, J., 1963: General circulation experiments with the primitive equations: I. The basic experiment. *Mon. Wea. Rev.*, **91**, 99–164.
- Smolarkiewicz, P. K., 1984: A fully multidimensional positive definite advection transport algorithm with small implicit diffusion. *J. Comput. Phys.*, **54**, 325–362.
- , and W. W. Grabowski, 1990: The multidimensional positive definite advection transport algorithm: Nonoscillatory option. *J. Comput. Phys.*, **86**, 335–375.
- , and P. J. Rasch, 1991: Monotone advection on the sphere: An Eulerian versus semi-Lagrangian approach. *J. Atmos. Sci.*, **48**, 793–810.
- , and L. G. Margolin, 1993: On forward-in-time differencing for fluids: Extension to a curvilinear framework. *Mon. Wea. Rev.*, **121**, 1847–1859.
- Spencer, R. W., 1993: Global oceanic precipitation from the MSU during 1979–91 and comparisons to other climatologies. *J. Climate*, **6**, 1301–1326.
- Sud, Y. C., and A. Molod, 1988: The roles of dry convection, cloud-radiation feedback processes and the influence of recent improvements in the parameterization of convection in the GLA GCM. *Mon. Wea. Rev.*, **116**, 11, 2366–2387.
- , and G. K. Walker, 1990: A review of recent research on improvement of physical parameterizations in the GLA GCM. *Physical Processes in Atmospheric Models*, D. R. Sikka and S. S. Singh, Eds., Wiley Eastern Ltd., 442–479.
- , and G. K. Walker, 1993: A rain evaporation and downdraft parameterization to complement a cumulus updraft scheme and its evaluation using GATE data. *Mon. Wea. Rev.*, **121**, 3019–3039.
- , P. J. Sellers, Y. Mintz, M. D. Chou, G. K. Walker, and W. E. Smith, 1990: Influence of the biosphere on the global circulation and the hydrologic cycle—A GCM simulation experiment. *For. Meteor.*, **52**, 133–179.
- , W. C. Chao, and G. K. Walker, 1991: Contributions to the implementation of Arakawa–Schubert cumulus parameterization in the GLA GCM. *J. Atmos. Sci.*, **48**, 1573–1586.
- Takacs, L. L., 1988: Effects of using a posteriori method for the conservation of integral invariants. *Mon. Wea. Rev.*, **116**, 525–545.
- , and R. Balgovind, 1983: High latitude filtering in global grid point models. *Mon. Wea. Rev.*, **111**, 2005–2015.
- Thuburn, J., 1993: Use of a flux-limited scheme for vertical advection in a GCM. *Quart. J. Roy. Meteor. Soc.*, **119**, 469–487.
- Tokioka, T., K. Yamazaki, A. Kitoh, and O. T. Ose, 1988: The equatorial 30–60 day waves and the Arakawa–Schubert cumulus parameterization. *J. Meteor. Soc. Japan*, **66**, 883–900.
- van Leer, B., 1977: Toward the ultimate conservative difference scheme. IV: A new approach to numerical convection. *J. Comput. Phys.*, **23**, 276–299.
- , 1979: Toward the ultimate conservative difference scheme. V: A second order sequel to Godunov’s method. *J. Comput. Phys.*, **32**, 101–136.
- Williamson, D. L., 1990: Semi-Lagrangian moisture transport in the NMC spectral model. *Tellus*, **42A**, 413–428.
- , and P. J. Rasch, 1989: Two-dimensional semi-Lagrangian transport with shape preserving interpolation. *Mon. Wea. Rev.*, **117**, 102–129.
- Woodward, P. R., and P. Colella, 1984: The numerical simulation of two-dimensional fluid flow with strong shocks. *J. Comput. Phys.*, **54**, 115–173.
- Xue, M., and A. J. Thorpe, 1991: A mesoscale numerical model using the nonhydrostatic pressure-based sigma-coordinate equations: Model experiments with dry mountain flows. *Mon. Wea. Rev.*, **119**, 1168–1185.
- Xue, Y. K., P. J. Sellers, J. L. Kinter III, and J. Shukla, 1991: A simplified biosphere model for global climate studies. *J. Climate*, **4**, 345–364.
- Zalesak, S. T., 1979: Fully multidimensional flux-corrected transport algorithms for fluid. *J. Comput. Phys.*, **31**, 335–362.